Geoderma 429 (2023) 116264

Contents lists available at ScienceDirect

Geoderma

journal homepage: www.elsevier.com/locate/geoderma

Quantification of the effects on the flow velocity caused by gramineous plants in the loess plateau in North-Western China

Youdong Cen [a,b], Kuandi Zhang [a,b,*], Yong Peng [c], Matteo Rubinato [d], Hongyang Zhang [a,b], Haixin Shang [a,b], Pu Li [a,b]

[a] State Key Laboratory of Soil Erosion and Dryland Farming on the Loess Plateau, Northwest A&F University, Yangling, Shaanxi, China
[b] Key Laboratory of Agricultural Soil and Water Engineering of Ministry of Education in Arid Areas, Northwest A&F University, Yangling, Shaanxi, China
[c] School of Natural and Built Environment, Queen's University Belfast, BT9 5AG, UK
[d] Centre for Agroecology, Water and Resilience, Ryton Gardens, Wolston Lane, Ryton-on-Dunsmore, Coventry University, CV8 3LG, UK

ARTICLE INFO

Handling Editor: Morgan Cristine L.S.

Keywords:
Flow velocity
Vegetation coverage
Manning equation
Flow regime
Overland flow

ABSTRACT

Accurate prediction of the mean velocity of overland flow is the premise and foundation for establishing a soil erosion model, but it is difficult to accurately estimate the mean flow velocity with the presence of vegetation. To explore the variation law of the mean velocity of overland flow under the influence of gramineous plants typical in the Loess Plateau in North-Western China, indoor scouring tests with ten levels of vegetation coverage (9.42 %–94.25 %), seven unit discharges (0.278–1.667 $L{\cdot}m^{-1}{\cdot}s^{-1}$), and five slope gradients (4°–12°) were performed. The results showed that the mean flow velocity initially increased and then decreased with an increase in vegetation coverage, and the critical cover was affected by the unit discharge. For a slope of 4°, the mean flow velocity with a vegetation coverage of 94.25 % was only 21.6 %–32.0 % of that on a bare slope, indicating that vegetation can effectively reduce flow velocity. For each experiment conducted, with an increase in vegetation coverage, the overland flow gradually moved from laminar flow to transitional flow. Based on the principle of equivalent roughness and Manning's equation, a prediction model was also established in order to predict more accurately the mean velocity associated with overland flow, and it has been validated against the experimental results demonstrating a satisfactory agreement with the measured values (adj.R^2 = 0.879, *NSE* = 0.867). These results provide further insights regarding the influence that the vegetation can have on the flow velocity and contribute to develop a better management of these environmental areas.

1. Introduction

Soil erosion, which is a major environmental problem worldwide, is an important factor that causes environmental deterioration (Yang et al., 2020). Studies conducted to date have shown that vegetation cover is an effective method for controlling soil erosion and plays an important role in soil and water conservation (Zhao et al., 2015; Rahma et al., 2017; Mu et al., 2019; Shao et al., 2020; Luo et al., 2020; Revell et al., 2022). Vegetation changes the hydrological conditions of runoff above the land surface, which affects the soil erosion process. On one hand, vegetation changes the physical properties of soil aggregates and improves the shear strength of soil (Gyssels and Poesen, 2003; Li and Pan, 2018). On the other hand, vegetation changes the flow characteristics and hydraulic properties of overland flow, thereby changing the mechanism of hydraulic erosion (Zhang et al.,2022). These are the reasons why multiple studies have been focusing on the estimation and characterisation of the mean flow velocity as a key parameter for describing the hydrodynamic characteristics of overland flow (Maji et al., 2020; Wang et al., 2019a; Wang et al., 2019b; D'Ippolito et al., 2021; Wang et al., 2020; Huai et al., 2021).

Previous studies have shown that vegetation can reduce flow velocities (Pan and Shangguan, 2006; Fu et al., 2019; Mu et al, 2019). In a movable-bed scouring test, Pan and Shangguan (2006) found that mean flow velocity decreased with an increase in vegetation coverage; compared with the bare slope, the flow velocity on the slope with vegetation decreased by approximately 50 %. Fu et al. (2019) and Mu et al. (2019) reached the same conclusion and found that the relationship between flow velocity and vegetation coverage decreased monotonically, however, Bouma et al. (2007) found that soil erosion also occurred because of the increase in vegetation and confirmed that,

* Corresponding author at: State Key Laboratory of Soil Erosion and Dryland Farming on the Loess Plateau, Northwest A&F University, Yangling, Shaanxi, China.
E-mail address: zhangkuandi428@126.com (K. Zhang).

https://doi.org/10.1016/j.geoderma.2022.116264
Received 13 June 2022; Received in revised form 21 October 2022; Accepted 10 November 2022

relative to low-density patches, high-density patches showed more erosion at the sides parallel to the main flow direction. Outside the vegetation patches, van Wesenbeeck et al. (2008) observed small trenches; in other words, soil erosion occurred too. At the same time, Zong and Nepf (2010) found that turbulent flows increased in vegetation patches with small coverage compared to those in patches with no coverage. Balke et al. (2012) also observed similar experimental phenomena. This evidence shows that, under certain conditions, with increasing vegetation, the mean flow velocity may increase, resulting in hydraulic erosion. These different findings indicate that the relationship between mean flow velocity and vegetation was affected by different behaviors of the vegetation. On one hand, the flow velocity usually decreases with increasing vegetation coverage when the vegetation is evenly distributed. On the other hand, the flow velocity may locally increase with increasing vegetation coverage when the behavior is arranged in vegetation patches that can promote preferential flow lines and, consequently, erosion. Therefore, further investigation of the relationship between flow velocity and vegetation coverage is needed and would be helpful for understanding the role of vegetation relative to the hydrodynamic characteristics of the overland flow.

The accurate calculation of the mean flow velocity is very crucial (Lei et al., 2010; Ali et al., 2012). Previous studies have found that the mean flow velocity can be predicted by the power function of the discharge (Govers, 1992; Nearing et al., 1999); which is calculated as follows:

$$u = aQ^b \tag{1}$$

In this equation, a and b are coefficients related to the underlying surface conditions, and Q is the discharge. Eq. (1) considers the mean velocity as a power function of discharge; but in fact, mantles on the land surface and slope gradients also affect flow velocity. The influence of the slope gradients on the flow velocity is affected by the shape of the underlying surface because different bed surface shapes have different resistance to overland flow. Abrahams et al. (1996) found that slope gradients significantly affected flow velocity and suggested that slope gradients are as important as discharge for controlling flow velocity. Takken and Govers (2000), investigating vegetation on a slope, suggested that the prediction results of Eq. (1) were not satisfactory, and that for more complex slope surface conditions, the credibility of the predictions will be lower if only the discharge was used to predict the flow velocity; thus, the influence of slope gradients should be considered. In another study, Al-Hamdan et al. (2012) found that when vegetation was low, the mean flow velocity was significantly correlated with the slope gradient. However, the dependence of the flow velocity on the slope gradient also increased with a decrease in the rough elements. In contrast, Polyakov et al. (2018) found that the correlation between mean flow velocity and slope gradient was poor and not statistically significant. Bond et al. (2020) obtained similar conclusions from their field observation experiments. In summary, according to the existing results identified within the literature, flow resistance on mobile beds is not affected by the slope while flow resistance on fixed beds is affected by the slope. Therefore, it is unreasonable to predict mean velocity under vegetation conditions using only the discharge. Thus, other studies have been conducted to calculate the mean velocity of overland flow based on the computational theory of hydraulics (Jin et al., 2000; Fu et al., 2019). For instance, Jin et al. (2000) conducted experimental research on shallow overland flow in the filter belt of non-submerged vegetation and derived a formula based on Manning's equation for the mean flow velocity:

$$u = \left(\frac{2g}{C_d D}\right)^{1/2} S^{1/2} \tag{2}$$

where g is the acceleration due to gravity, C_d is the drag coefficient of the vegetation, S is the hydraulic gradient, and D represents the vegetation density per unit width, $D = \frac{\sum A}{hL}$, A is the upstream surface area in front of vegetation, L is the length of the control volume, h is the mean water depth. In Eq. (2), the value of C_d is considered to be 1 (Jin et al., 2000). In fact, C_d is a function of the Reynolds number (Wang et al., 2015). However, Jin et al. (2000) did not discuss the applicability of this calculation model to different flow regimes because Eq. (2) is derived from Manning's equation, and Manning's equation is generally not applicable to the laminar flow regime (Kirstetter et al., 2016); therefore, this model is not commonly used. Based on Manning's equation, Fu et al. (2019) derived a model of mean flow velocity through multivariate nonlinear regression analysis, which is as follows:

$$u = \frac{1}{\left(\alpha + \beta(1 - e^{-0.061 C_v})^{1.668}\right) h^{0.604 - 0.710 e^{-0.219 C_v}}} S^{0.5} h^{2/3} \tag{3}$$

where α and β are coefficients. Although Eq. (3) indicates a quantitative relationship between vegetation and mean flow velocity, the equation has no rigorous theoretical basis for determining the Manning coefficient. In addition, the equation may be limited by different experimental conditions; therefore, it is not representative because Manning's equation is generally applicable only to turbulent conditions. When the overland flow is within the laminar regime, the drag component from the bed surface may not be constant (Helmers and Eisenhauer, 2006).

In summary, the influence of vegetation on flow velocity has not yet been fully clarified, and the relationships between variables involved within this interaction require a further understanding which must be quantitatively studied. Moreover, the application scope of different flow velocity calculation models should be clearly stated. To address this gap and contribute with additional information, this study has the following objectives: 1) to study the effects caused by gramineous plants in the Loess Plateau in North-Western China on mean flow velocity under specific scenarios, 2) establish a new calculation model for the mean flow velocity based on Manning's equation; and 3) compare the prediction accuracy and applicable conditions of different flow velocity calculation equations. The findings of this study will contribute to enlarging the existing knowledge linked to the influence of vegetation on hydraulic characteristics and broaden the application scope of existing soil erosion models.

2. Materials and methods

2.1. Experimental apparatus

A water supply device consisting of a constant water tank and a steady flow device was employed (Fig. 1). The constant water tank was 2 m in length, 1 m in width, and 0.5 m in height. To maintain flow stability, two steady flow plates with grids were installed parallel to the flow direction in the front section of the experimental flume; they helped eliminate the influence of inlet flow disturbance. In addition, a thermometer with an accuracy of 0.1 °C was placed in the steady flow device to record the water temperature. The flume size was 4.5 m in length, 0.3 m in width, and 0.1 m in height. The truss-supporting and slope-adjusting devices were arranged under the flume. The device for regulating discharge included ball valves for large-range flow regulation (0–40 L·min^{-1}) on the constant water tank and a peristaltic pump for small-range flow regulation (0–20 L·min^{-1}).

2.2. Experimental design

After the implementation of the Grain for Green Project, the vegetation coverage of the Loess Plateau has been significantly improved (Fu et al., 2011; Mu et al., 2012; Gu et al., 2020). According to the research and investigation of Liu et al. (2012), the dominant species on the Loess Plateau are gramineous vegetation. To date, many studies have been carried out around gramineous vegetation (Pan et al., 2016; Liu et al., 2012; Ding and Li, 2016; Fu et al.,2019; Shang et al., 2020). Therefore, this study mainly considers the impact of gramineous vegetation on

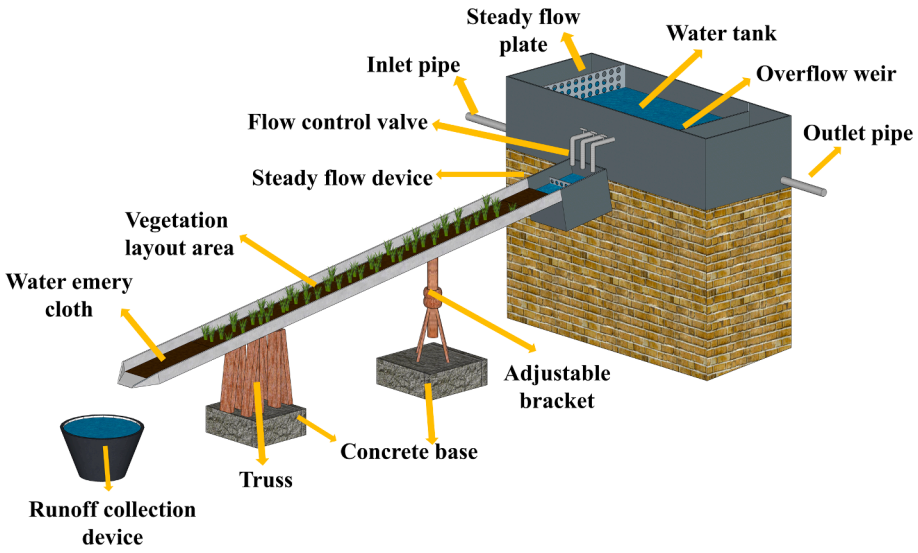

Fig. 1. Schematic of the experimental setup.

overland flow hydraulic characteristics linked with the process of vegetation restoration. Clusters of artificial grass with 1 mm-thick stems and heights of 15 mm were used to simulate the influence of common gramineous plants on runoff in the Loess Plateau in North-Western China. As shown in Fig. 3, an artificial grass was fixed by 55 needle-shaped cylindrical rods on the pedestal. The pedestal is a thin plate with a thickness of 3 mm. Its shape is round and its diameter is 20 mm. A 40-mesh sandpaper with a roughness of 0.38 mm was secured on the bottom of the experimental flume to simulate the roughness of the natural underlying surface. The vegetation was distributed in a patch pattern, as shown in Fig. 2. Considering the wide range of coverage changes during vegetation restoration (Shang et al., 2020), a blank control group and ten coverage levels were set, as shown in Table 1. The research of Shang et al. (2020) found that the slope gradient of the water erosion zone on the Loess Plateau is generally below 10°, and the overland flow is the main factor causing water erosion (Guo et al., 2019). When the slope gradient is greater than 15°, the main erosion type on the slope is gravity erosion (Xu et al., 2020; Ma et al., 2021). This study mainly considers the influencing factors of hydraulic erosion. Therefore, the maximum slope gradient of 12° is adopted in this study, and five slope gradients (4°, 6°, 8°, 10°, and 12°) were used. Moreover, torrential rainfall recorded on the Loess Plateau varied between 30 and 120 mm h^{-1} (Shang et al., 2020), and 60 min was chosen as the rainfall duration with a catchment area of 10 m^2 (Cen et al.,2022). Therefore, seven unit discharges (0.278, 0.417, 0.556, 0.833, 1.111, 1.389, and 1.667 $L{\cdot}m^{-1}{\cdot}s^{-1}$) and were used.

2.3. Experimental measurements

The water depth and the flow velocity were measured by measuring needle and dye ($KMnO_4$) tracing in our experiment. There was a big error in measuring velocity with dye under the condition of vegetation cover because the vegetation disturbed the diffusion of dye and made it difficult to capture its centroid (Zhang et al.,2010). Firstly, the vegetation would also interfere with the vertical velocity profile (Ali et al.,2012). In addition, the measurement result of surface velocity was doubtful due to the error of velocity measurement means (Abrahams et al.,1996; Myers,2002). On the contrary, the flow cannot infiltrate in the fixed-bed experiment, so the water depth did not change along the way, which means that the water depth was not affected by the spatial distribution. The flow discharges were constant during the experiment, so the water depth was not affected by time. This means that the water depth was constant in time and space distribution and was easy to measure, so the mean velocity was calculated by water depth in our experiments.

There were four observation sections along the longitudinal direction of the flume; from top to bottom along the slope surface, four sections were positioned at 0 + 1.25 m, 0 + 1.75 m, 0 + 2.25 m, and 0 + 2.75 m, and the distribution range of vegetation cover was 0 + 0.75–0 + 3.25 m. Flow discharge, slope gradient, and vegetation coverage were

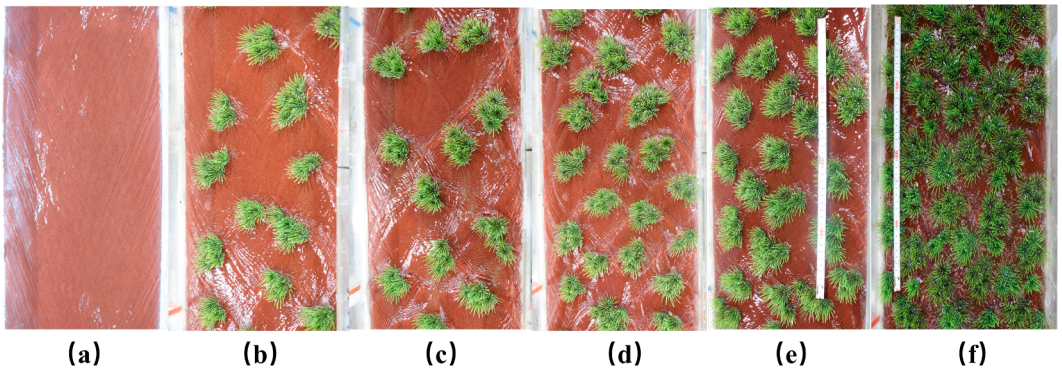

Fig. 2. Two test schemes were used for the experiments: bare slope in (a) and vegetation from (b) to (f). The different vegetation coverages of each test area surface in the flume are: 9.42% (b), 18.85% (c), 47.12% (d), 56.55% (e), and 84.82% (f). Grasses were arranged randomly in clusters; small cover was used to form a large canopy projection area.

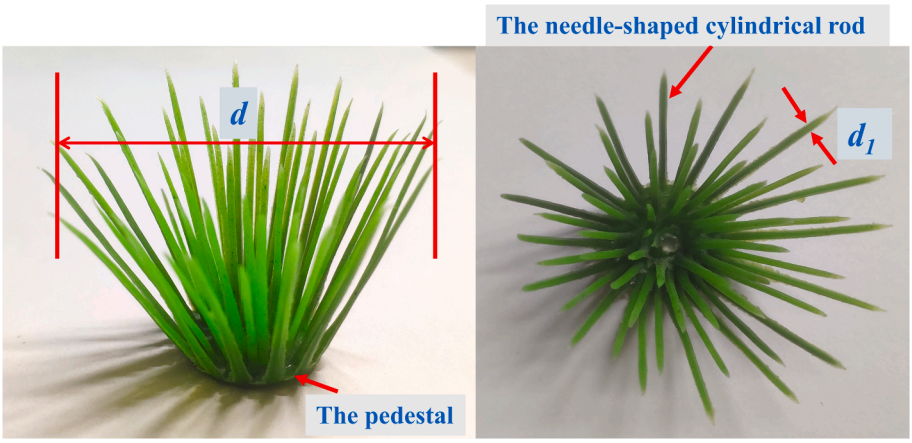

Fig. 3. The sketch of artificial grass.

Table 1
Test parameters for different treatments.

Treatment	The number of grass clusters	Stem density (%)	Coverage (%)	Unit discharge ($L \bullet m^{-1} \bullet s^{-1}$)	Slope (°)	Mean flow velocity ($m \bullet s^{-1}$)	Water depth (mm)
Control group	0	0	0	0.278–1.667	4°–12°	0.117–0.446	1.83–4.84
T1	100	0.37	9.42	0.278–1.667	4°–12°	0.129–0.533	1.94–3.24
T2	200	0.73	18.85	0.278–1.667	4°–12°	0.127–0.442	1.80–4.86
T3	300	1.10	28.27	0.278–1.667	4°–12°	0.142–0.471	1.49–6.30
T4	400	1.47	37.70	0.278–1.667	4°–12°	0.119–0.383	1.34–7.08
T5	500	1.83	47.12	0.278–1.667	4°–12°	0.123–0.360	1.75–8.52
T6	600	2.20	56.55	0.278–1.667	4°–12°	0.118–0.353	1.85–10.53
T7	700	2.57	65.97	0.278–1.667	4°–12°	0.104–0.285	1.97–11.61
T8	800	2.93	75.40	0.278–1.667	4°–12°	0.083–0.253	2.22–12.86
T9	900	3.30	84.82	0.278–1.667	4°–12°	0.077–0.232	2.37–13.97
T10	1000	3.67	94.25	0.278–1.667	4°–12°	0.066–0.213	2.65–15.71

adjusted to designated values before each experiment. In each run, the flow discharge was measured at the flume outlet using a volumetric method. After the discharge was stabilised to the design discharge and the water levels were stable, three measuring points were selected from each cross-section to measure the water depth using a water level measuring needle with an accuracy of 0.01 mm. The following steps were then performed: 1) take the mean of water depths at the three measuring points as the mean water depth of the respective section; 2) measure the water depth of the four sections; and 3) check whether the discharge matched the design discharge again after the measurement was completed, which is to prevent other factors from interfering with the test during the measurement process. If the error between the test discharge and the design discharge exceeded ± 5 %, it was necessary to measure the water depth again. Finally, the mean water depth of all sections was taken as the mean water depth of the flume. The water temperature t during the test was recorded using a water tank thermometer to calculate the kinematic viscosity coefficient of the water flow. The discharge, the slope gradient, and the coverage degree were changed in turn, repeating the above operations until all tests were completed.

2.4. Parameter calculation

Vegetation coverage (C_v) is an important parameter to quantitatively reflect the vegetation growth status, which has an important impact on ecosystem functions such as water and soil conservation, wind prevention, and sand fixation, and is mostly used to monitor the long-term change characteristics of vegetation. In addition, in the field condition experiment, vegetation coverage is easier to obtain, so this paper selects vegetation coverage as a variable that affects the flow velocity. C_v was calculated by dividing the projected area of vegetation canopy by the area of the test plot. The formula to calculate it is listed below:

$$C_v = \frac{N\pi d^2}{4BL} \tag{4}$$

where N is the number of grass clusters in the experimental area and the values of N in different test treatments are shown in Table 1, and as shown in Fig. 3, d is the diameter of the grass cluster (0.03 m), B is the width of the test flume (0.3 m), and L is the length of the vegetation layout interval (2.5 m).

The mean velocity in the cross-section is expressed by:

$$u = \frac{Q}{1000hb_1} \tag{5}$$

where u is the mean velocity in the cross-section ($m \cdot s^{-1}$), Q is the discharge corresponding to the design discharge ($L \cdot s^{-1}$), h is the mean water depth of the section (m), b_1 represents the effective width except the space actually occupied by grass in this experiment (m), where $b_1 = B \times (1\text{-}D_v)$, and D_v is the vegetation density, which was calculated by dividing the sectional grass stem area by the plot area. The formula to calculate D_v is listed below:

$$D_v = \frac{55N\pi {d_1}^2}{4BL} \tag{6}$$

where d_1 is the diameter of the needle-shaped cylindrical rod (as shown in Fig.3, d1 = 1 mm). The values of D_v are listed in Table 1.

The Reynolds number, Re, can be calculated as follows:

$$Re = \frac{uR}{\nu_0} \tag{7}$$

where R is the hydraulic radius (m), ν_0 represents the kinematic viscosity coefficient of the water flow ($m^2 \cdot s^{-1}$), which is calculated according to the Poiseuille formula:

$$\nu_0 = \frac{0.01775}{(1 + 0.0337t + 0.00022t^2)} \tag{8}$$

The Froude number, *Fr*, can be calculated as follows:

$$Fr = \frac{u}{\sqrt{gh}} \tag{9}$$

where g is the acceleration of gravity, 9.81 m·s^{-2}.

2.5. Data analysis

The analysis of variance (ANOVA) is used to explore whether the unit discharge and slope gradient have a significant impact on the average flow velocity. *F* is a statistic of ANOVA. The larger the value of *F*, the more significant the difference between different treatments. It can be calculated by the following formula:

$$F = \frac{SSA/p - 1}{SSE/n - p} \tag{10}$$

where *SSA* is the sum of squares regression,$SSA = \sum_{j=1}^{n_l}\sum_{i=1}^{n_j}(\overline{X}_j - \overline{X})^2$, $\overline{X}_j$ is the average value of the sample at level A_j, $\overline{X}$ is the average of all samples, *SSE* is the sum of squares error,$SSE = \sum_{j=1}^{n_l}\sum_{i=1}^{n_j}(X_{ij} - \overline{X}_j)^2$, X_{ij} is the value of the sample at level A_j, p is the number of independent variables and n is the number of samples.

We choose the relative root mean square error (*RRMSE*), the corrected correlation coefficient (adj.R^2), and the Nash-Sutcliffe coefficient (*NSE*) to test the applicability of the model. The *RRMSE* is the ratio of the standard error to the observed value, which can well evaluate the prediction effect of the model, and is calculated by the following formula:

$$RRMSE = \frac{\sqrt{(1/n)\sum_{i=1}^{n}(O_i - P_i)^2}}{\overline{O}} \tag{11}$$

where O_i is the measured value of the flow velocity, P_i is the predicted value of flow velocity, and $\overline{O}$ is the mean observed value of flow velocity.

The adj.R^2 is calculated according to the following equation as follows:

$$R^2 = \frac{\left[\sum_i^n (O_i - \overline{O})(P_i - \overline{P})\right]^2}{\sum_{i=1}^n (O_i - \overline{O})^2 \sum_{i=1}^n (P_i - \overline{P})^2} \tag{12}$$

$$adj.R^2 = 1 - \left(1 - R^2\right)\frac{n-1}{n-p-1} \tag{13}$$

where $\overline{P}$ is the mean predicted value of the flow velocity.

The *NSE* is an index used to evaluate the simulation results of hydrological models, and its numerical value can reflect the deviation between the calculated and measured values. The formula to obtain it can be written as follows:

$$NSE = 1 - \frac{\sum_{i=1}^n (O_i - P_i)^2}{\sum_{i=1}^n (O_i - \overline{O})^2}. \tag{14}$$

2.6. Theoretical analysis of mean flow velocity model

In this study, based on the principle of equivalent roughness, combined with Manning's equation and the characteristics of overland flow movement, a model for the mean flow velocity with vegetation was established. This method assumes that the resistance of the rough bed without vegetation is equal to the form resistance of the vegetation stems when on the slope. In other words, the influence of form resistance caused by vegetation stems is the same as that caused by the shear stress of the rough underlying surface without vegetation (Kim et al., 2012; Wang et al., 2015).

Manning's equation is a common formula for calculating the flow velocity of an open channel and is defined as follows:

$$u = \frac{1}{n}R^{2/3}S^{1/2} \tag{15}$$

In this equation, n is the Manning coefficient, S is the hydraulic gradient, where $S = \sin\theta$ under experimental conditions, and θ is the inclination angle of the flume. According to the force analysis, the main forces on the overland flow with vegetation are the resistance caused by vegetation F_D, bed shear stress F_b, and effective gravity of the water body along the moving direction F_G. A force diagram is shown in Fig. 4a.

Assuming that the overland flow is uniform, according to the principle of mechanical balance (Jin et al.,2000):

$$F_b + F_D = F_G \tag{16}$$

The equations for the bed shear stress and the detouring flow resistance of the vegetation can be listed as follows (Huai et al., 2021):

$$F_b = \gamma R S B_1 L = \frac{\gamma u^2 n_0^2}{R^{1/3}} B_1 L \tag{17}$$

$$F_D = \frac{\gamma C_d A_i u^2}{2g} \tag{18}$$

where γ is the specific weight of the flow, B_1 is the width of flow not affected by the drag force of vegetation. At this time, the artificial grass is considered as a cylinder with diameter *d*. $B_1 = B(1 - C_v)$, where B is the flume width (0.3 m), n_0 is the Manning roughness coefficient for a bare slope (0.029), C_d is the drag force coefficient, A_i is the upstream surface area in front of vegetation, $A_i = Ndh$. The detouring flow resistance of the vegetation was evenly distributed on the bed surface, and an equivalent cross section of overland flow was obtained, as shown in Fig. 4b.

In the vegetation section of the flume, calculations of the water volume V before the equivalence process and the water volume V_e after the equivalence process are as follows:

$$V = BLh(1 - C_v) \tag{19}$$

$$V_e = BLh_e \tag{20}$$

where V_e is the equivalent water volume in the vegetation area after the equivalence process, and h_e is the equivalent water depth. According to the conservation law of fluid mass, the water volume is unchanged before and after the equivalence process, and h_e is calculated by the simultaneous solution equation:

$$h_e = h(1 - C_v) \tag{21}$$

The discharge is unchanged by the equivalence process and is expressed as follows:

$$u_e h_e B = uhB_1 \tag{22}$$

Thus,

$$u_e = u \tag{23}$$

Equivalent bed shear stress F_{eb} is calculated by:

$$F_{eb} = \gamma R_e S B L = \frac{\gamma u_e^2 n_e^2}{R_e^{1/3}} BL \tag{24}$$

where R_e is the equivalent hydraulic radius, and n_e is the equivalent Manning coefficient. According to the mechanical equilibrium equation:

$$F_{eb} = F_G \tag{25}$$

By solving Eq. (16) and Eq. (25) simultaneously, we obtain:

$$F_{eb} = F_b + F_D \tag{26}$$

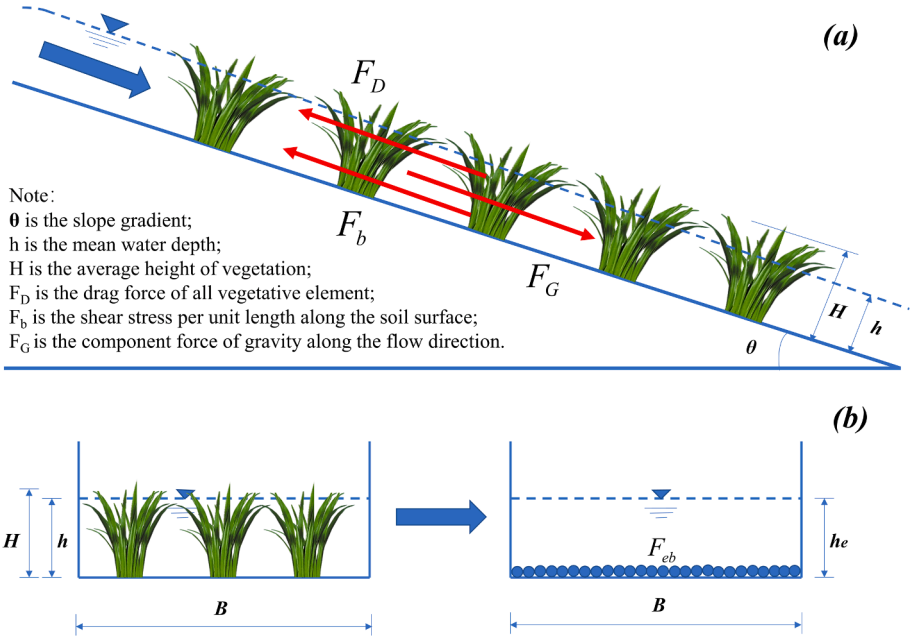

Fig. 4. Flow force diagram (a), and schematic of the equivalent roughness (b).

$$\frac{\gamma u_e^2 n_e^2}{R_e^{1/3}} BL = \frac{\gamma u^2 n_0^2}{R^{1/3}} B_1 L + \frac{\gamma C_d N d h u^2}{2g} \tag{27}$$

Solving and simplifying Eq. (27), we find:

$$n_e = \sqrt{\left(\frac{R_e}{R}\right)^{1/3} n_0^2 (1 - C_v) + R_e^{1/3} C_d \frac{2hC_v}{\pi dg}} \tag{28}$$

Substituting the above equation into Eq. (15), using $R_e = f(R, C_v)$, and simplifying, we obtain:

$$u = \frac{f(R, C_v)^{0.5} S^{0.5}}{\sqrt{\frac{n_0^2(1-C_v)}{R^{1/3}} + C_d \frac{2hC_v}{\pi dg}}} \tag{29}$$

where C_d is related to the flow regime and vegetation morphology. In theory, R_e can be calculated according to water depth (h), vegetation coverage (C_v), and the width of the test flume (B). However, this definition is based on the assumption of equivalent roughness. Whether this assumption is consistent with the actual situation needs to be verified by test data. At the same time, Manning's equation needs to calculate the flow velocity according to the hydraulic radius R, but the definition of R_e does not directly reflect the relationship between R_e and R, and the relationship between R_e and R is affected by vegetation coverage (C_v). To sum up, we assume a functional relationship between R_e and R, C_v, and verify this relationship through experimental data.

3. Results

3.1. Establishment of the mean flow velocity model

From the theoretical analysis of the mean flow velocity model, a general formula was obtained for calculating the mean water velocity, as shown in Eq. (29). Since the mean flow velocity model needs to be developed and validated with experimental data, we randomly split the experimental data into two datasets. One dataset was used to obtain the parameters in Eq. (29), such as C_d; the other dataset was used to test the accuracy of the established model. In addition, in order to make the test results more representative, the established model was also tested on the dataset of Ding and Li (2016). Based on the data set used to develop the model, the established model is as follows:

$$u = \frac{kR^{0.5} S^{0.5}}{C_v^{0.1} \sqrt{\frac{n_0^2(1-C_v)}{R^{1/3}} + C_d \frac{2hC_v}{\pi dg}}} \tag{30}$$

$$C_d = 1838 \frac{C_v^{0.665} S^{0.248}}{Re^{0.887}} \tag{31}$$

In this study, $k = 0.7$, Eq. (31) was obtained by multiple regression analysis, and C_d was a function of the Re. In addition, C_d was also affected by the vegetation and slope gradient. As shown in Fig. 5, the predicted value of the mean flow velocity obtained using Eq. (30) is evenly distributed on both sides of the 1:1 line. Based on the data set used to validate the model, the t and F tests showed that the model was significant at a level of 0.05, and as shown in Table 2, the test statistics of this model are adj.$R^2 = 0.879$, $NSE = 0.867$, and $RRMSE = 0.151$, which shows that the model can verify the results of this experiment and has high prediction accuracy. For the test results of Ding and Li (2016), $k = 0.6$. The t and F tests showed that the model was significant at a level of 0.05, and the adj.$R^2 = 0.700$, $NSE = 0.704$, and $RRMSE = 0.123$, indicating that the model is also suitable for moving bed erosion and sediment-laden flow.

In order to compare the applicability of Eq. (30) and Eq. (1), Eq. (2), and Eq. (3), the specific expressions of Eq. (1), Eq. (2), and Eq. (3) are obtained based on the data set used to develop the model in this experiment (Table 2). As shown in Table 2 and Fig. 5, when the validation dataset is used to test Eq. (1), Eq. (2), and Eq. (3), the three equations all show unsatisfactory prediction accuracy. Eq. (1) only uses unit discharge to predict the mean flow velocity, and the test statistics of Eq. (1) are adj.$R^2 = 0.307$, $NSE = 0.237$, and $RRMSE = 0.255$; Eq. (2) ignores the influence of the roughness of the underlying surface on the flow velocity, and the test statistics of Eq. (2) are adj.$R^2 = 0.577$, $NSE = 0.299$, and $RRMSE = 0.314$; Manning coefficient in Eq. (3) is obtained through multiple nonlinear regression analysis, and the test statistics of Eq. (3) are adj.$R^2 = 0.307$, $NSE = 0.237$, and $RRMSE = 0.255$. Therefore, compared against the above three equations, Eq. (30), that was developed on the basis of equivalent roughness and Manning's equation, has wider applicability.

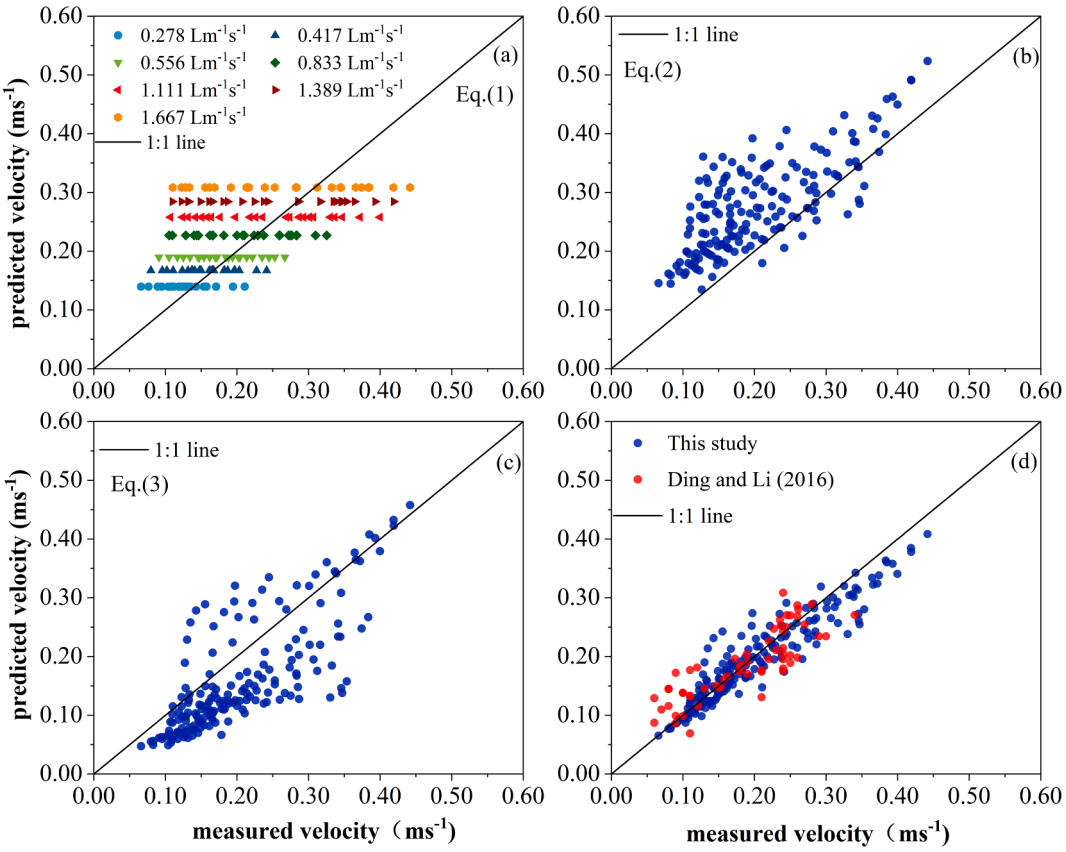

Fig. 5. Compare the different predicted equations.

Table 2
Statistics between the different predicted equations.

	Prediction equations	Adj.R^2	NSE	RRMSE	N
Eq.(1) (Govers, 1992)	$u = 0.246q^{0.442}$	0.307	0.237	0.255	175
Eq.(2) (Jin et al.,2000)	$u = \left(\frac{2g}{C_d D}\right)^{0.5} S^{0.5}$	0.577	0.299	0.314	175
Eq.(3) (Fu et al.,2019)	$u = \frac{S^{0.5}h^{0.667}}{\left(0.008 + 1.875(1 - e^{-0.061C_v})^{1.668}\right)h^{0.604-0.710e^{-0.219C_v}}}$	0.307	0.237	0.255	175
This study	$u = \frac{0.7R^{0.5}S^{0.5}}{C_v^{0.1}\sqrt{\frac{n_0^2(1-C_v)}{R^{1/3}} + C_d\frac{2hC_v}{\pi dg}}}$	0.879*	0.867*	0.151	175

Notes: [a] * represents that it is significant at the level of 0.05. N is the number of data sets.

[b] C_d can be calculated by this formula: $C_d = 1838\frac{C_v^{0.665}S^{0.248}}{Re^{0.887}}$.

3.2. Influence of different experimental factors on mean flow velocity

3.2.1. Distribution of mean flow velocity under different conditions

The distribution of the mean flow velocity was affected by the unit discharge and slope gradient as it is possible to observe in Fig. 6. At the slope of 4 °, 6 °, 8 °, 10 °, and 12 °, for the range of unit discharges between 0.278 and 1.667 L·m^{-1}·s^{-1}, the mean flow velocity is 0.066–0.380, 0.083–0.430, 0.104–0.460, 0.108–0.523, 0.109–0.533 m·s^{-1} respectively, and the extreme difference is 0.314, 0.347, 0.356, 0.415 and 0.424 m·s^{-1} respectively. To summarise this effect, it is possible to state that with the increase in unit discharge, the extreme difference in the mean flow velocity for different vegetation coverages also increased. According to the results of ANOVA (Table 3), at a confidence level of 0.05, the influence of unit discharge on the mean flow velocity was significantly different for different slope gradient conditions ($P < 0.05$). At the slope of 4 °, 6 °, 8 °, 10 °, and 12 °, F is 6.225,8.507,10.618,13.868, and 19.250 respectively, indicating that with an increase in the slope gradient, the influence of the unit discharge on the mean flow velocity became increasingly significant. Using the same method of variance analysis, it was found that the influence of slope gradient on mean flow velocity also differed significantly ($P < 0.05$).

3.2.2. Effect of vegetation coverage on mean flow velocity

The relationship between mean flow velocity and vegetation coverage is similar under all unit discharge and slope gradient conditions. Therefore, in order to make the manuscript more concise and the research results representative, the maximum (1.667 L·m^{-1}·s^{-1}), minimum (0.278 L·m^{-1}·s^{-1}), and two intermediate values (0.556 and 1.111 L·m^{-1}·s^{-1}) for unit discharge and the maximum (12°), minimum (4°),

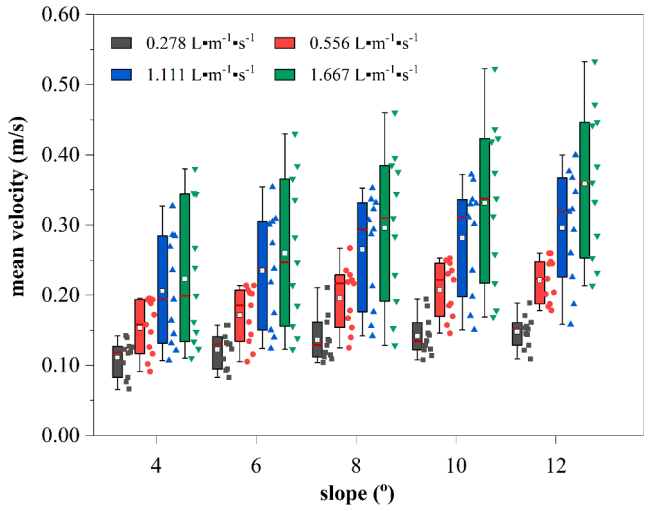

Fig. 6. Characteristics of mean velocity distribution under various discharges and slope gradients.

Table 3
The statistical parameters of ANOVA.

	Source	*SS*	*df*	*MS*	*F*	*P*
4 °	*q*	0.087	3	0.029	6.225	0.001
	error	0.187	40	0.005		
	total	0.275	43			
6 °	*q*	0.128	3	0.043	8.507	0.000
	error	0.200	40	0.005		
	total	0.328	43			
8 °	*q*	0.168	3	0.056	10.618	0.000
	error	0.211	40	0.005		
	total	0.379	43			
10 °	*q*	0.229	3	0.076	13.868	0.000
	error	0.220	40	0.006		
	total	0.449	43			
12 °	*q*	0.276	3	0.092	19.250	0.000
	error	0.191	40	0.005		
	total	0.467	43			

Note: *SS* is the sum of squares, *df* is the degree of freedom, and *MS* is the mean squares.

and an intermediate value (8°) for slope gradient was chosen to analyze the effect of vegetation coverage on mean flow velocity. For each unit discharge, the mean flow velocity initially increased and then decreased as density increased, and the relationship was affected by the unit discharge (Fig. 7). When the unit discharge was 0.278 $L{\cdot}m^{-1}{\cdot}s^{-1}$ and the slopes were 4°, 8°, and 12°, the mean flow velocity reached a maximum value at T3, T4, and T3, respectively, increasing from 21.2 % to 53.8 % compared with that in the control group (Fig. 7a). Then, with an increase in density, the mean flow velocity began to decrease. When the unit discharge was 1.667 $L{\cdot}m^{-1}{\cdot}s^{-1}$, under the three slope gradients, the mean flow velocity peaked at T1 (Fig. 7d), indicating that the inflection point of the mean flow velocity in the change process shifted to lower values of coverage with increasing unit discharge. Compared with the control group ($C_v = 0$), when the vegetation coverage increased to 94.25 % (T10), the mean flow velocity decreased by 24.2 % – 43.8 %, 31.3 % – 51.7 %, 56.0 % – 62.6 % and 52.2 % – 68.0 %, respectively, for the four unit discharges (0.278, 0.556, 1.111, and 1.667 $L{\cdot}m^{-1}{\cdot}s^{-1}$). The analysis showed that for larger unit discharges under non-submerged conditions, vegetation had a more significant effect on the mean flow velocity.

3.2.3. *Effect of the unit discharge and slope on the mean flow velocity*

The mean flow velocity increased with an increase in the unit discharge and slope gradient, but its change rate was more significantly affected by vegetation (Fig. 8). Without vegetation on the slope, when the unit discharge increased from 0.278 to 1.667 $L{\cdot}m^{-1}{\cdot}s^{-1}$, the range of mean flow velocity increased from 0.130 to 0.152 to 0.344–0.446 $m{\cdot}s^{-1}$. When the slope gradient increased from 4° to 12°, the mean velocity increased by 28.4 % to 37.7 %. When the vegetation coverage was 94.25 %, with an increase in the unit discharge, the mean flow velocity increased from 0.066 to 0.109 to 0.115–0.203 $m{\cdot}s^{-1}$, which were 21.6 % to 32.0 % and 25.7 % to 44.6 % of those for the bare slope, respectively, indicating that the increase in vegetation can effectively inhibit the increase in mean flow velocity. When the slope gradient increased from 4° to 12°, the mean flow velocity increased from 57.5 % to 72.6 %.

To investigate the quantitative relationship among mean flow velocity, unit discharge, and slope gradient, a multivariate nonlinear regression analysis was performed using the SPSS software. The functional relationships under different vegetation conditions are presented in Table 4. The slope gradient exponent reflects the influence of the slope gradient on the mean flow velocity. Except for the T1 treatment ($C_v = 9.42$ %), other treatments are greater than the control group ($C_v = 0$). With the increase in vegetation, the slope gradient exponent gradually increased and remained at 0.5 after coverage condition T6, indicating that the increase in vegetation can increase the contribution of slope gradient to flow velocity, but the maximum value of slope gradient exponent can only be close to 0.5. The discharge exponent reflects the contribution of the unit discharge to the flow velocity. When vegetation covered the slope surface, the discharge exponent decreased from 0.703 to 0.214, indicating that the increase in vegetation weakened the contribution of unit discharge to the flow velocity. Satisfactory fitting relationships were obtained under different vegetation conditions, and the adj.R^2 values were all greater than 0.85 (Table 4). However, when this relationship was applied to all data, the prediction effect of the formula was very poor (adj.$R^2 = 0.478$), indicating that it is inaccurate to use only the unit discharge and slope gradient to predict the flow velocity, which reflects the necessity of considering vegetation.

3.3. *Effect of vegetation coverage, slope gradient, and unit discharge on flow regime*

By using *Re* and *Fr* to divide the flow regime directly, the relationship between flow velocity and water depth during the regime transition cannot be found intuitively. Occasionally, the change characteristics among the hydraulic factors were the focus of our attention. Therefore, the logarithmic coordinates of the flow velocity and water depth can be considered for flow regime division. With *lgh* and *lgu* as the independent and dependent variables, respectively, the test data were plotted with double logarithmic coordinate axes.

Re was used extensively to define flow regimes, and characterise the relationship between *Re* and flow resistance in terms of the Darcy–Weisbach resistance coefficient (*f*). The relationship between *f* and *Re* is different when *Re* is in different ranges. For open channel flow (Powell,2014), when $Re < 500$, *f* is only a function of *Re*, at this time, the flow viscosity is dominant. When $Re > 2000$, *f* is mainly affected by the bed surface roughness, at this time, the flow inertia force is dominant. Due to different movement characteristics and influencing factors of open channel flow and overland flow, their flow resistance laws are also different. For overland flow, when $Re < 580$, *f* is only a function of *Re*, at this time, the flow viscosity is dominant (Wang et al., 2019a; Wang et al., 2019b). When $Re > 5000$, *f* is mainly affected by the bed surface roughness, and at this time, the flow inertia force is dominant (Zhang et al., 2012). Considering that the test conditions are similar to those of Wang et al. (2019a,b) and Zhang et al.(2012), we set $Re = 580$, $Re = 5000$, and $Fr = 1$ so that the boundary of the water flow regime division can be obtained in the double logarithmic coordinates of *h* and *u* (Fig. 9).

The overland flow can be regarded as a two-dimensional flow because its water depth is very small, and the hydraulic radius *R* is approximately equal to the average water depth *h* of the section (Li et al.,1996; Zhao et al.,2015; Pan et al.,2016). Therefore, the relationship between *h* and *u* is linear for a given *Re*. As shown in Fig. 9, there

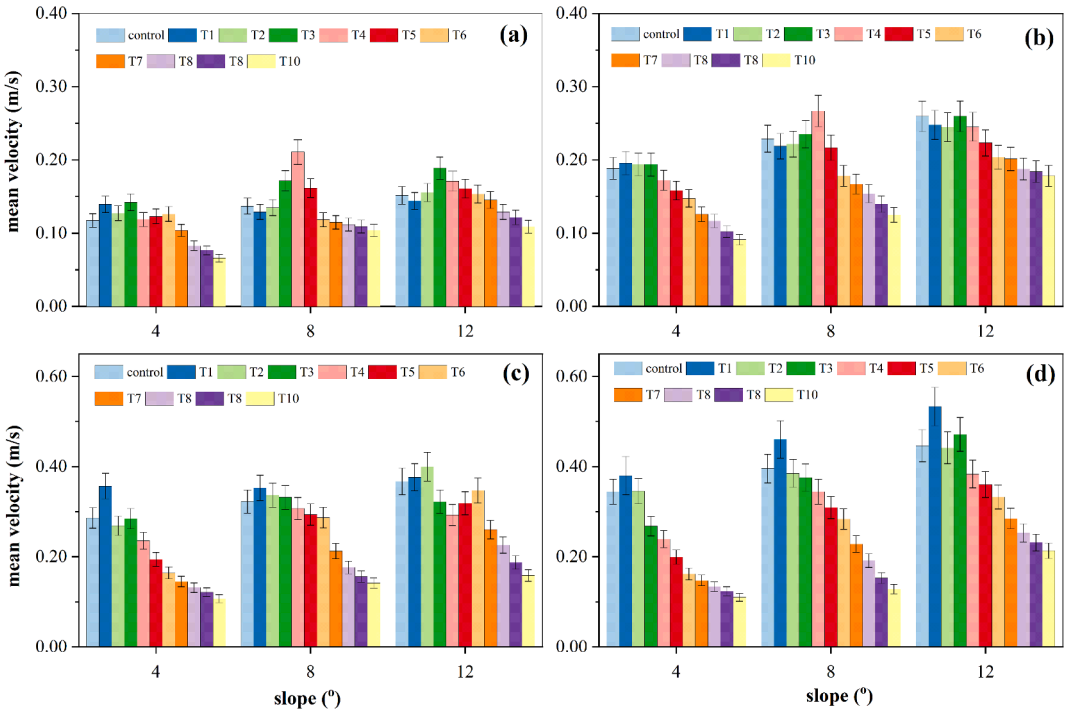

Fig. 7. Variation of the mean flow velocity with vegetation coverage Cv, and the unit discharges are 0.278, 0.556, 1.111, and 1.667 L·m-1·s-1 from (a) to (d), respectively.

was a positive correlation between mean flow velocity and mean water depth with a gradual increase in unit discharge. Under various slope gradient conditions, when the unit discharge reached 0.188 $L{\cdot}m^{-1}{\cdot}s^{-1}$, *Re* changed to 580, and the water flow reached the transitional flow regime. At this time, the mean velocity increased more slowly, and the mean water depth increased more quickly, indicating that the increase in unit discharge can extend the water flow to the transitional flow regime. When the slope gradient increased from 4° to 12°, the velocity range of the flow entering the transitional flow regime ranged from 0.129 to 0.238 $m{\cdot}s^{-1}$, and the water depth ranged from 0.239 to 0.472 cm. As the slope gradient increased, the mean velocity increased, while the mean water depth decreased, which was more likely to cause soil erosion.

From Fig. 9, on the premise of unchanging vegetation and slope gradient, with the increase of unit discharge, it was found that the mean velocity and mean water depth were increasing, and the flow transitioned from the laminar to the transitional flow regime; when the discharge and slope gradient remain unchanged, with the increase of vegetation, the water flow gradually transitioned from supercritical to subcritical flow; when the other conditions remain unchanged, with the increase of slope gradient, the flow gradually extended from subcritical to supercritical flow.

4. Discussion

This study investigated the effect on the flow velocity caused by gramineous plants in the Loess Plateau in North-Western China. Through the immovable bed scouring test, the variation laws between vegetation cover, unit discharge, slope gradient, and mean flow velocity were investigated. A prediction model of mean flow velocity with vegetation was established based on the principle of equivalent roughness and Manning's equation. The effects of vegetation coverage and slope gradient on mean flow velocity will be discussed in sections 4.1 and 4.2. Moreover, the mean velocity prediction model will be further analyzed in section 4.4.

4.1. Effect of vegetation coverage on mean flow velocity

This study found that the mean flow velocity did not have a single correlation with vegetation, but there were different correlations for different vegetation conditions, and the correlations were also affected by the unit discharge. In this study, the mean velocity increased initially with the increase in vegetation, reached a peak, and then decreased, while the increase of unit discharge would reduce the critical vegetation coverage threshold that makes the mean flow velocity reach the maximum value. This conclusion has been reflected in field observations (Bouma et al., 2007; Zong and Nepf, 2010; Balke et al., 2012), and combined with the results of the immovable bed experiment and field observations from this study, it can be stated that vegetation changed the movement boundary of overland flow, the wetted area of water flow, and the conditions of the underlying slope surface. Vegetation can occupy part of the channel space, which means that the space of overland flow is compressed; thus, flow aggregates and exits through the gap between vegetation. Moreover, owing to the decrease in wetted area, the mean flow velocity increases. With the increase in vegetation coverage, the flow direction will change and it is no longer a straight line (Fig. 10). Moreover, the change of flow direction is more complex, and the flow path is also longer. As a result, the drag force on the flow increases, and more energy is consumed. In our experiment, the mean flow velocity began to decrease with an increase in vegetation. Dunkerley (2001) considered that, with respect to the protruding obstacles in laminar flow, the mean flow velocity can increase or decrease with the change in obstacles. The actual condition depends on the geometric distribution pattern of the obstacles because the shrinking of the water flow path reduces the vegetation resistance, and as a result, the flow velocity increases.

In fact, the relationship between vegetation and mean flow velocity in this study seems to differ from the results obtained by Fu et al. (2019), which was mainly caused by the different conditions in the experimental design. In this study, the unit discharge was 0.278–1.667 $L{\cdot}m^{-1}{\cdot}s^{-1}$, while the unit discharge range of Fu et al. (2019) was 1.351–5.405 $L{\cdot}m^{-1}{\cdot}s^{-1}$. The minimum discharge of the experiment conducted by Fu

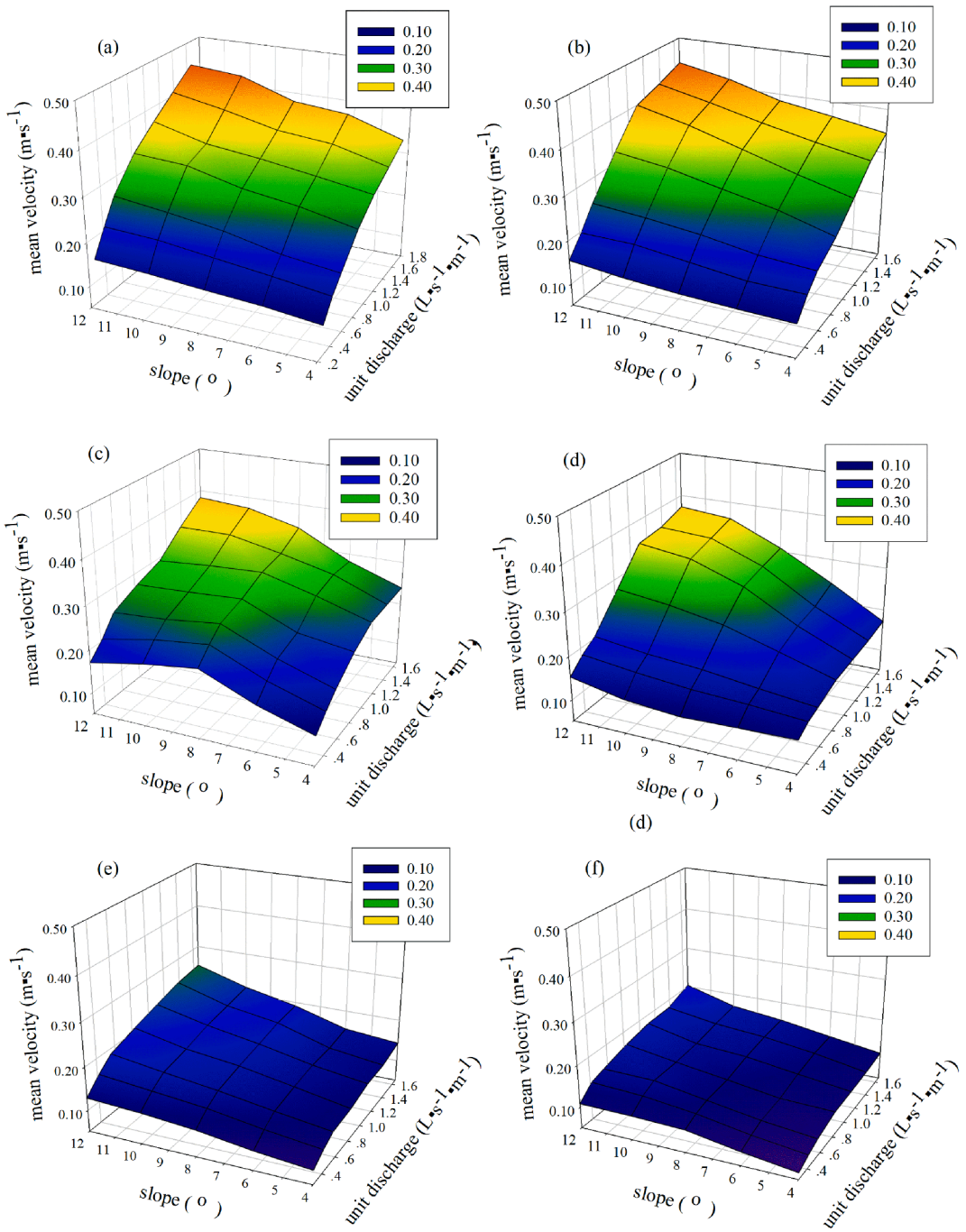

Fig. 8. The relationship among mean velocity, unit discharge, and slope gradients at different coverages, Cv are 0%, 18.85%, 37.70%, 56.55%, 75.40% and 94.25% from (a) to (f), respectively.

Table 4
Fitting formulas of the mean flow velocity, unit discharge, and energy slope for different model parameters.

Treatment	Fitting formula	adj.R^2	Treatment	Fitting formula	adj.R^2
Control group	$u = 0.501q^{0.555}S^{0.246}$	0.990	T6	$u = 0.711q^{0.426}S^{0.557}$	0.896
T1	$u = 0.478q^{0.703}S^{0.180}$	0.983	T7	$u = 0.553q^{0.331}S^{0.524}$	0.966
T2	$u = 0.546q^{0.447}S^{0.297}$	0.983	T8	$u = 0.470q^{0.286}S^{0.509}$	0.952
T3	$u = 0.531q^{0.562}S^{0.277}$	0.961	T9	$u = 0.422q^{0.229}S^{0.516}$	0.926
T4	$u = 0.521q^{0.347}S^{0.321}$	0.912	T10	$u = 0.380q^{0.214}S^{0.519}$	0.889
T5	$u = 0.590q^{0.374}S^{0.423}$	0.917	All	$u = 0.502q^{0.435}S^{0.364}$	0.478

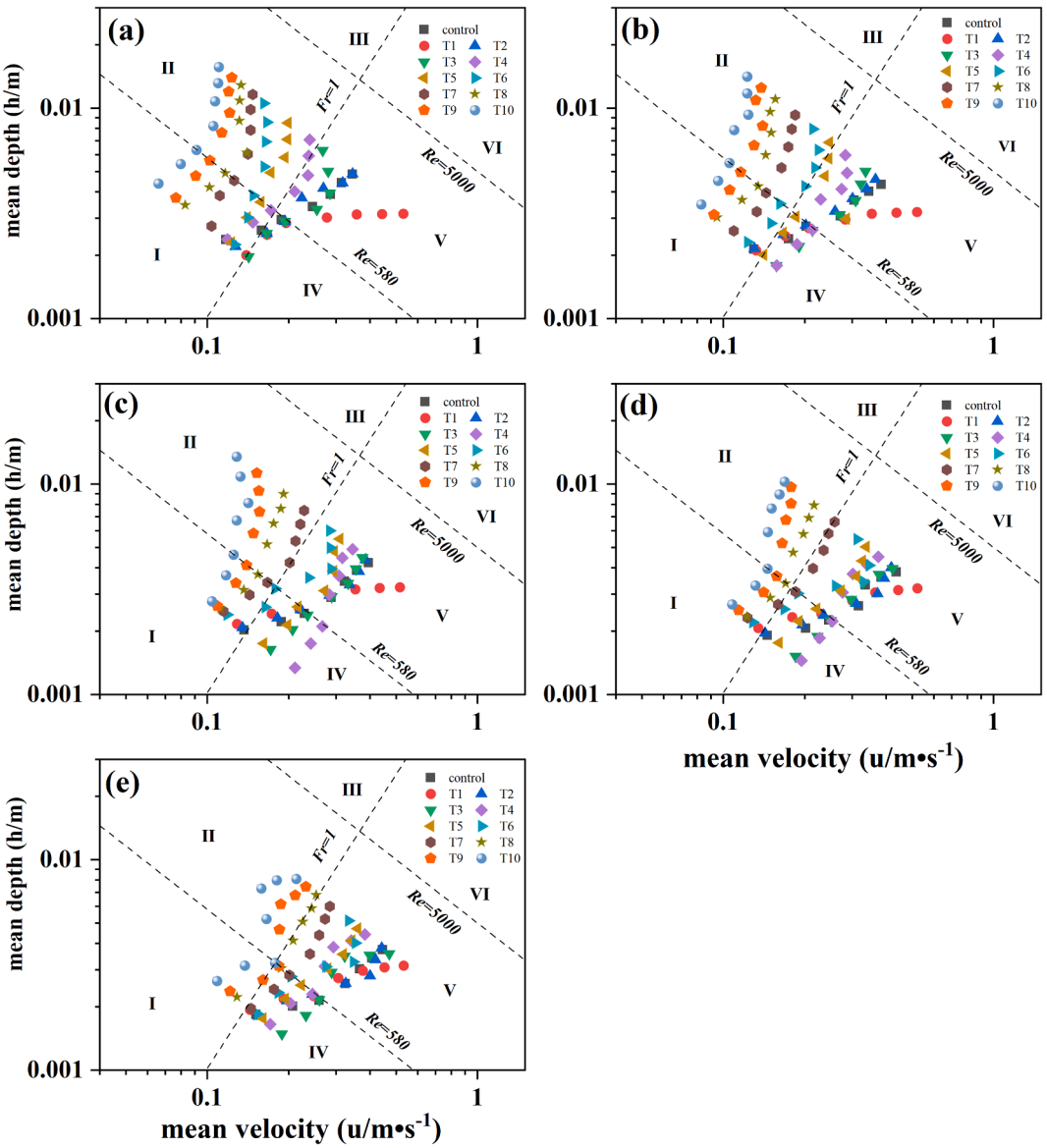

Fig. 9. Variation characteristics of mean velocity in different flow regimes. I = subcritical laminar flow (Re < 580 and Fr < 1), II = subcritical transitional flow (580 < Re < 5000 and Fr < 1), III = subcritical turbulent flow (Re > 5000 and Fr < 1), IV = supercritical laminar flow (Re < 580 and Fr > 1), V = supercritical transitional flow (580 < Re < 5000 and Fr > 1), and VI = supercritical turbulent flow (Re > 5000 and Fr < 1). The slope gradient values are 4°,6°,8°,10°, and 12° from (a) to (e), respectively.

et al. (2019) was very close to the maximum discharge of this test. At our maximum discharge, the mean flow velocity reached its peak at T1 and then decreased with an increase in vegetation. In addition, the grass cluster condition of this test differs from that of Fu et al. (2019), and the water obstructing surface area is also different; thus, under our study conditions, the relationship between mean flow velocity and vegetation was not monotonous. Pan and Shangguan (2006) found that the mean flow velocity decreased with an increase in vegetation, which is different from the results of this study. Compared with the results obtained by Pan and Shangguan (2006), in this experiment, the roughness of the underlying surface was unchanged, the shear stress of the bed surface was less than the form resistance caused by vegetation, and the change in water flow resistance depended on the change in vegetation. Therefore, differently from the movable bed test, vegetation is the main factor affecting the flow velocity in the fixed bed experiment. Compared with the fixed bed test, the movable bed test has more factors that can affect the flow velocity, such as the underlying surface roughness (Nicosia et al., 2020), microtopography (Li et al., 2021), and surface cover (Wang et al., 2015). Firstly, the rougher the underlying surface, the greater the resistance to flow (Nicosia et al., 2020). Secondly, the microtopography may cause the flow to consume more energy (Li et al., 2021). In addition, the surface cover can exert additional resistance to the flow, reducing its velocity. In summary, compared with the fixed bed test, the movable bed test provides greater resistance to overland flow. Thus, the flow velocity decreases due to greater resistance.

4.2. *Effect of slope gradient on mean flow velocity*

In this study, the slope gradient had a significant impact on the mean flow velocity, and the mean flow velocity increased with increasing slope gradient. Compared with previous studies, in the immovable bed test, the slope gradient could significantly affect the mean velocity, which is consistent with the view of Ban et al. (2017). However, the slope gradient was not the main factor affecting the mean flow velocity in the movable bed test, and the flow velocity could be predicted only according to the unit discharge. Polyakov et al. (2018) considered that in

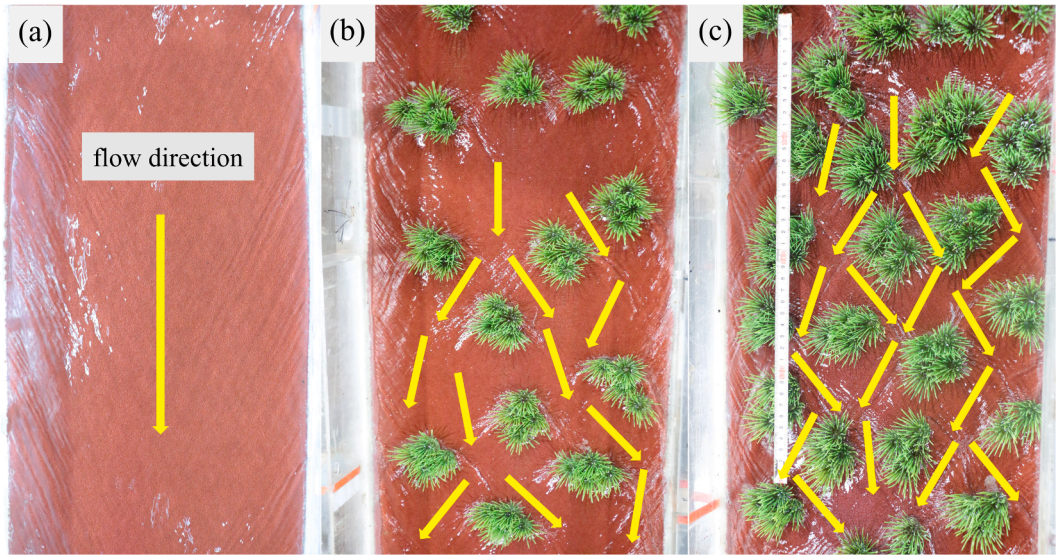

Fig. 10. The flow direction under different vegetation coverage. (a) $C_v = 0$; (b) $C_v = 18.85$ %; (c) $C_v = 75.40$ %.

the process of runoff erosion, the greater the slope gradient, the greater the surface roughness of the soil slope; they further suggested that the increased resistance counteracted the contribution of the slope gradient to the flow velocity, forming a dynamic feedback loop. Nearing et al. (2017) also confirmed this result. In this experiment, during the initial stage of hydraulic erosion, the increase in slope gradient led to an increase in flow velocity, which caused the soil surface to evolve into a steep slope area and produce greater hydraulic roughness to restrain the increase in flow velocity. As a result, the mean flow velocity gradually became independent of the slope gradient. That is, initially steep slopes with high velocity tended to form rougher surfaces, which would be expected to reduce the velocity and indirectly reduce the contribution of the slope gradient to the flow velocity. However, in the immovable bed test, the underlying surface of the flow was constant, and the gravity in the flow direction increased with the increasing slope gradient, which promoted the conversion of potential energy to kinetic energy and increased the mean flow velocity. In summary, since the increased flow velocity cannot change the underlying surface conditions, making the underlying surface rougher and thus reducing the flow velocity, the flow velocity increases with the slope gradient.

4.3. Effect of vegetation coverage on flow regime

Vegetation can change the flow regime transition law of overland flow, while the increase in vegetation limits the development of laminar to turbulent flow, which is consistent with the conclusions obtained by Shang et al. (2020). Under different vegetation coverage, discharge, and slope gradient conditions, the flow regime did not reach turbulent flow, but was primarily maintained at the laminar or transitional flow regimes. The "laminar flow regime" mentioned here mainly refers to the flow regime when the Reynolds number of the water flow is <580. Such a flow regime is significantly different from the laminar flow of an open-channel uniform flow. Thus, in order to emphasise its unique flow characteristics, some scholars have named it the "virtual laminar flow regime" (Wang et al., 2019b). The water flowed around the vegetation due to its obstruction, and the water level increased in the upstream surface area in front of the vegetation, while that downstream of the vegetation was lower than the mean water depth. Upstream of each vegetation cluster, the kinetic energy of the water flow was transformed into potential energy, forming stagnant waves on both sides of the vegetation. Meanwhile, the depth of water downstream of the vegetation decreased, and the flow streamline was a curve; simultaneously, vortices were formed. Previous research has shown that the flow velocity was affected by surface roughness, which is controlled by vegetation coverage (Bond et al., 2020). Additionally, the obstruction of vegetation reduces the flow velocity and increases the water depth, which inhibits the flow from becoming turbulent (Chen et al., 2015). In addition, the gravity component of the overland flow increases with the increase of the slope gradient, which increases the inertial force of the flow and accelerates the conversion of potential energy to kinetic energy. At this time, the flow velocity increases and the water depth decreases with the increase of slope gradient, resulting in the transition of overland flow from laminar to turbulent. From this experiment, the increase in unit discharge provided the source power for the transition of overland flow from laminar to transitional. The increase in vegetation hindered the flow regime transition from laminar to turbulent flow, while an increase in slope gradient reduced the contribution of vegetation to this transition.

4.4. Analysis of mean flow velocity prediction model

Based on the principle of equivalent roughness, according to Eq. (16), the equation for the equivalent Manning coefficient was derived, and the mean flow velocity calculation model was obtained. According to Eq. (29), the roughness coefficient is composed of the shear stress caused by the boundary roughness and the drag force caused by the vegetation. The resistance caused by the vegetation was related to vegetation, water depth, and flow regime, which is similar to the conclusion from Jin et al. (2000). However, Jin et al. (2000) considered that, under non-submerged conditions, the increase in water depth had minimal impact on the mean velocity; thus, the influence of water depth could be ignored in the model, which differs from our experimental results. By comparison, this may have been caused by differences in vegetation morphology, as Jin et al. (2000) used cylindrical polypropylene bristles to simulate vegetation in their experiment, which are simple in structure and have no divergence in space. In contrast, we used artificial gramineae vegetation, and its umbrella shape changed the vertical velocity distribution of the water flow; as the water depth increased, the flow resistance increased, and the umbrella shape could drag the vegetation more effectively. Therefore, this model did not ignore the influence of the water depth change on the flow velocity, making the model more applicable. Fu et al. (2019) suggested that the relationship between the Manning coefficient and water depth conforms to the power function rate. Although some scholars have obtained such results in similar experiments (Wu, 2008; Mügler et al., 2011), the mechanism underlying this relationship needs further exploration, and

whether the velocity model obtained by multivariate analysis is universally applicable must be verified. According to Eq. (30), when the water depth increased, the wet perimeter increased and the vegetation form resistance increased, which in this experiment, increased the flow resistance, revealing the quantitative relationship between water depth and the Manning coefficient to some extent. The velocity model in this study considers the variation in the drag force coefficient under different *Re* values and obtains the equation of the drag force coefficient, which is helpful for understanding the composition and variation of flow resistance.

Eq. (30) shows that the mean flow velocity increased with an increase in $R^{0.5}$ and $S^{0.5}$ and decreased with an increase in the total flow resistance. The total flow resistance is composed of boundary and vegetation form resistances, which supports the conclusion of Shang et al. (2020). The boundary resistance is affected by vegetation and hydraulic radius; with an increase in these parameters, the proportion of boundary resistance is reduced, and its effect on flow velocity is small. Thus, Eq. (2) ignores boundary resistance. The resistance of the vegetation morphology increased with an increase in the drag force coefficient C_d, water depth h, and coverage C_v. According to the experimental results, the drag force coefficient can be expressed as a power function of the vegetation, water depth, and *Re*. Eq. (31) shows that C_d increases with C_v and decreases with *Re*, which supports the conclusions of Wang et al. (2015) and Cheng et al. (2019).

Eq. (1) only predicted the flow velocity through unit discharge, which ignores the influence of vegetation coverage, slope gradient, underlying surface roughness, and other factors on the flow velocity, so the prediction accuracy was low when predicting the flow velocity (Fig. 5a). Compared with Eq. (1), Eq. (30) comprehensively considered the effects of vegetation coverage, slope gradient, and underlying surface roughness on flow velocity, which broadens the application scope of Eq. (30). Eq. (2) ignored the influence of the underlying surface roughness on the flow velocity, which leads to an overestimation of the flow velocity (Fig. 5b). Compared with Eq. (2), Eq. (30) clarified that the influence of boundary resistance on the mean velocity is as important as that of vegetation form resistance, which cannot be ignored in this calculation, and the method of the drag force coefficient C_d was proposed. This is helpful in expanding the application range of Eq. (30) and improving the accuracy of the velocity prediction. Manning's coefficient in Eq. (3) has specific conditions for use, and the parameters need to be re-calibrated when used under different test conditions, which is a limitation of nonlinear regression analysis. Compared with Eq. (3), Eq. (30) clarified the composition of the Manning coefficient for vegetation, which is composed of the boundary and vegetation form resistances and is helpful in better understanding the Manning coefficient, indicating that the hydraulic radius with vegetation is a function of vegetation coverage and water depth. In addition, for the data set of Ding and Li (2016), the coefficient k in Eq. (30) is 0.6, while for the data set of this test, k is 0.7, and this may be due to the impact of rainfall, sediment-laden flow, and movable bed conditions.

4.5. Limitations and future research prospects

Simulated immovable bed scouring tests were performed to accurately investigate the influence of vegetation on the mean flow velocity. To eliminate the interference of bed conditions and flow sediment, the influence of moving bed erosion and sediment-laden flow on the average velocity was not considered. The sandpaper with a roughness of 0.38 mm was secured on the bottom of the test flume to simulate natural underlying surface roughness, which is close to the median particle size of loess (Wu et al., 2017). Although Eq. (30) could verify the results of Ding and Li (2016), the model we developed did not quantify the effects of litter and microtopography on flow velocity in detail. The differences between artificial and natural vegetation lie in both litter, microtopography and spatially variable infiltration rates. The underlying surface conditions and soil properties were affected by the litter and the downslope often experiences a larger flow discharge than the upslope due to the cumulative effect of slope runoff, which was caused by the spatially variable infiltration rates (Shang et al.,2020). Furthermore, the influence of litter, micro-topography, and spatially variable infiltration rates on the flow velocity needs to be further discussed in future research. In addition, because the experimental flow did not reach the turbulent regime, to further expand the applicability of Eq. (30), the new data are necessary for calibration and testing to develop the overland flow velocity equation.

Vegetation in rivers and watercourses significantly affect velocity profiles and it is crucial to better characterize these effects to address the societal needs such as flood management, river management, soil erosion protection and ecosystems restoration. Furthermore, vegetation is believed to be a sustainable solution to characterise natural channel processes and features therefore its presence can be beneficial to remove environmental threats on streams, rivers and the surrounding riparian areas. Taking into account that climate change is expected to change temperatures within natural environments, the growth of vegetation may differ in the future and it is crucial to be able to predict the effect that vegetation has in order to judge the benefits and the costs of its presence within natural environments, including watercourses. Therefore, this study is another contribution to provide further insights to seek better management of these environmental areas.

5. Conclusions

To investigate the influence of gramineous plants in the Loess Plateau in North-Western China on the mean velocity of overland flow, indoor scouring experiments were conducted for ten patch patterns of vegetation, seven unit discharges, and five slopes, and the variation laws of the mean velocity for different vegetation coverages were discussed. The main conclusions obtained by this study are as follows:

(1) The mean flow velocity firstly increased and then decreased with increasing vegetation coverage, and its peak inflection point decreased with an increase in unit discharge, while the slope gradient had a significant impact on the mean flow velocity, which should be considered fully in the mean flow velocity prediction model.
(2) For this study, the flow was maintained within the laminar and transitional flow regimes. With increasing vegetation coverage, the overland flow gradually moved from supercritical to subcritical flow. Then, the flow velocity decreased, and the effect on soil erosion was reduced, which indicates that an increase in vegetation coverage can effectively prevent the occurrence of water and soil loss, as expected.
(3) Based on the principle of equivalent roughness and Manning's equation, a model for the mean flow velocity with vegetation was established. In this study, the mean flow velocity decreased with an increase in the boundary and vegetation form resistances, and the mean flow velocity increased with an increase in $R^{0.5}$ and $S^{0.5}$. The predicted velocity was in agreement with the measured value (adj.$R^2 = 0.879$, $NSE = 0.867$, $RRMSE = 0.151$). Because the flow did not reach the turbulent regime, the use of the mean flow velocity prediction model in the turbulent flow regime must still be verified by the new data.

Data Availability

All data used during the study are available from the corresponding author by request.

Declaration of Competing Interest

The authors declare that they have no known competing financial interests or personal relationships that could have appeared to influence the work reported in this paper.

Data availability

Data will be made available on request.

Acknowledgments

This research was financially supported by the National Natural Science Foundation of China [grant numbers 41877076, 52179079]; the State Key Laboratory of Soil Erosion and Dryland Farming on the Loess Plateau [grant number A314021402-202108].

References

Abrahams, A., Li, G., Parsons, A., 1996. Rill Hydraulics on semi-arid hillslope, southern Arizona. Earth surface processes Landforms 21, 35–47. https://doi.org/10.1002/(SICI)1096-9837(199601)21:13.0.CO;2-T.

Al-Hamdan, O.Z., Pierson, F.B., Nearing, M.A., Stone, J.J., Williams, C.J., Moffet, C.A., Kormos, P.R., Boll, J., Weltz, M.A., 2012. Characteristics of concentrated flow hydraulics for rangeland ecosystems: implications for hydrologic modeling. Earth Surface Processes and Landforms 37 (2), 157–168. https://doi.org/10.1002/esp.2227.

Ali, M., Sterk, G., Seeger, M., Stroosnijder, L., 2012. Effect of flow discharge and median grain size on mean flow velocity under overland flow. Journal of Hydrology 452–453, 150–160. https://doi.org/10.1016/j.jhydrol.2012.05.051.

Balke, T., Klaassen, P.C., Garbutt, A., van der Wal, D., Herman, P.M.J., Bouma, T.J., 2012. Conditional outcome of ecosystem engineering: A case study on tussocks of the salt marsh pioneer Spartina anglica. Geomorphology 153–154, 232–238. https://doi.org/10.1016/j.geomorph.2012.03.002.

Ban, Y., Lei, T., Gao, Y., Qu, L., 2017. Effect of stone content on water flow velocity over Loess slope: non-frozen soil. Journal of Hydrology 549, 525–533. https://doi.org/10.1016/j.jhydrol.2017.03.069.

Bond, S., Kirkby, M.J., Johnston, J., Crowle, A., Holden, J., 2020. Seasonal vegetation and management influence overland flow velocity and roughness in upland grasslands. Hydrological Processes 34 (18), 3777–3791. https://doi.org/10.1002/hyp.13842.

Bouma, T.J., van Duren, L.A., Temmerman, S., Claverie, T., Blanco-Garcia, A., Ysebaert, T., Herman, P.M.J., 2007. Spatial flow and sedimentation patterns within patches of epibenthic structures: Combining field, flume and modelling experiments. Continental Shelf Research 27 (8), 1020–1045. https://doi.org/10.1016/j.csr.2005.12.019.

Cen, Y.D., Zhang, K.D., Peng, Y., Rubinato, M., Liu, J.J., Ling, P., 2022. Experimental study on the effect of simulated grass and stem coverage on resistance coefficient of overland flow. Hydrological Processes 36 (10), e14705. https://doi.org/10.1002/hyp.14705.

Chen, Y., Liu, X., Wang, X., et al., 2015. Effects of roughness elements distribution on overland flow resistance. Journal of Mountain Science 15 (5), 1145–1156. https://doi.org/10.1007/s11629-014-3391-8.

Cheng, N.S., Hui, C.L., Chen, X., 2019. Estimate of Drag Coefficient for a Finite Patch of Rigid Cylinders. Journal of Hydraulic Engineering. 145 (2), 06018019.1–06018019.5.

D'Ippolito, A., Calomino, F., Alfonsi, G., Lauria, A., 2021. Flow Resistance in Open Channel Due to Vegetation at Reach Scale: A Review. Water 13, 116. https://doi.org/10.3390/w13020116.

Ding, W., Li, M., 2016. Effects of grass coverage and distribution patterns on erosion and overland flow hydraulic characteristics. Environmental Earth Sciences 75 (6), 1–14. https://doi.org/10.1007/s12665-016-5329-7.

Dunkerley, D., 2001. Estimating the mean speed of laminar overland flow using dye injection-uncertainty on rough surfaces. Earth Surface Processes and Landforms 26 (4), 363–374. https://doi.org/10.1002/esp.185.

Fu, B., Liu, Y., Lü, Y., He, C., Zeng, Y., Wu, B., 2011. Assessing the soil erosion control service of ecosystems change in the Loess Plateau of China. Ecological Complexity 8 (4), 284–293. https://doi.org/10.1016/j.ecocom.2011.07.003.

Fu, S., Mu, H., Liu, B., Yu, X., Liu, Y., 2019. Effect of plant basal cover on velocity of shallow overland flow. Journal of Hydrology 577, 123947. https://doi.org/10.1016/j.jhydrol.2019.123947.

Govers, G., 1992. Relationship between discharge, velocity and flow area for rills eroding loose, non-layered materials. Earth Surface Processes and Landforms 17 (5), 515–528. https://doi.org/10.1002/esp.3290170510.

Gu, C., Mu, X., Gao, P., Zhao, G., Sun, W., Tan, X., 2020. Distinguishing the effects of vegetation restoration on runoff and sediment generation on simulated rainfall on the hillslopes of the loess plateau of China. Plant and Soil 447 (1–2), 393–412. https://doi.org/10.1007/s11104-019-04392-4.

Guo, H., Zhang, B., Hill, R.L., Wu, S., Zhang, K., 2019. Fish-scale pit effects on erosion and water runoff dynamics when positioned on a soil slope in the loess plateau region, china. Land Degradation and Development 30 (15), 1813–1827. https://doi.org/10.1002/ldr.3379.

Gyssels, G., Poesen, J., 2003. The importance of plant root characteristics in controlling concentrated flow erosion rates. Earth Surface Processes and Landforms 28 (4), 371–384. https://doi.org/10.1002/esp.447.

Helmers, M.J., Eisenhauer, D.E., 2006. Overland flow modeling in a vegetative filter considering non-planar topography and spatial variability of soil hydraulic properties and vegetation density. Journal of Hydrology 328 (1–2), 267–282. https://doi.org/10.1016/j.jhydrol.2005.12.026.

Huai, W.X., Li, S., Katul, G.G., Liu, M.Y., Yang, Z.H., 2021. Flow dynamics and sediment transport in vegetated rivers: A review. Journal of Hydrodynamics 33, 400–420. https://doi.org/10.1007/s42241-021-0043-7.

Jin, C.X., Römkens, M.J.M., Griffioen, F., 2000. Estimating manning's roughness coefficient for shallow overland flow in non-submerged vegetative filter strips. Transactions of the Asae, 43(6): 1459-1466. 10.13031/2013.3044.

Kim, J., Ivanov, V.Y., Katopodes, N.D., 2012. Hydraulic resistance to overland flow on surfaces with partially submerged vegetation. Water Resources Research 48 (10), W10540. https://doi.org/10.1029/2012wr012047.

Kirstetter, G., Hu, J., Delestre, O., Darboux, F., Lagrée, P.Y., Popinet, S., Fullana, J.M., Josserand, C., 2016. Modeling rain-driven overland flow: Empirical versus analytical friction terms in the shallow water approximation. Journal of Hydrology 536, 1–9. https://doi.org/10.1016/j.jhydrol.2016.02.022.

Lei, T., Chuo, R., Zhao, J., Shi, X., Liu, L., 2010. An improved method for shallow water flow velocity measurement with practical electrolyte inputs. Journal of Hydrology 390 (1–2), 45–56. https://doi.org/10.1016/j.jhydrol.2010.06.029.

Li, G., Abrahams, A.D., Atkinson, J.F., 1996. Correction factors in the determination of mean velocity of overland flow. Earth Surface Processes and Landforms 21 (6), 509–515. https://doi.org/10.1002/(SICI)1096-9837(199606)21:63.0.CO;2-Z.

Li, C., Pan, C., 2018. The relative importance of different grass components in controlling runoff and erosion on a hillslope under simulated rainfall. Journal of Hydrology 558, 90–103. https://doi.org/10.1016/j.jhydrol.2018.01.007.

Li, P., Zhang, K., Wang, J., Feng, D., 2021. Response of interrill erosion to flow parameters of sand loess in regions with high and coarse sediment yields. Journal of Hydrology 592, 125786. https://doi.org/10.1016/j.jhydrol.2020.125786.

Liu, Y., Fu, B.J., Lv, Y.H., Wang, Z., Gao, G.Y., 2012. Hydrological responses and soil erosion potential of abandoned cropland in the loess plateau, china. Geomorphology 138 (1), 404–414. https://doi.org/10.1016/j.geomorph.2011.10.009.

Luo, J., Zhou, X., Rubinato, M., Li, G., Tian, Y., Zhou, J., 2020. Impact of multiple vegetation covers on surface runoff and sediment yield in the small basin of Nverzhai, Hunan Province, China. Forests 11 (3), 329. https://doi.org/10.3390/f11030329.

Ma, Y.L., Xu, X.Z., Xiao, P.Q., Yan, Q., Zhao, C., 2021. Geomorphic natural hazard on loess terrain: expansion on the gully sidewall. Natural Hazards 2021 (109), 2535–2555. https://doi.org/10.1007/s11069-021-04931-2.

Maji, S., Hanmaiahgari, P.R., Balachandar, R., Pu, J.H., Ricardo, A.M., Ferreira, R.M.L., 2020.A. Review on Hydrodynamics of Free Surface Flows in Emergent Vegetated Channels. Water 12, 1218. https://doi.org/10.3390/w12041218.

Mu, H., Yu, X., Fu, S., Yu, B., Liu, Y., Zhang, G., 2019. Effect of stem basal cover on the sediment transport capacity of overland flows. Geoderma 337, 384–393. https://doi.org/10.1016/j.geoderma.2018.09.055.

Mu, X., Zhang, X., Shao, H., Gao, P., Wang, F., Jiao, J., Zhu, J., 2012. Dynamic changes of sediment discharge and the influencing factors in the Yellow River, China, for the recent 90 years. CLEAN–Soil. Air, Water 40, 303–309. https://doi.org/10.1002/clen.201000319.

Mügler, C., Planchon, O., Patin, J., Weill, S., Silvera, N., Richard, P., Mouche, E., 2011. Comparison of roughness models to simulate overland flow and tracer transport experiments under simulated rainfall at plot scale. Journal of Hydrology 402 (1–2), 25–40. https://doi.org/10.1016/j.jhydrol.2011.02.032.

Myers, T.G., 2002. Modeling laminar sheet flow over rough surfaces. Water Resources Research. 38 (11), 1230. https://doi.org/10.1029/2000WR000154.

Nearing, M.A., Simanton, J.R., Norton, L.D., Bulygin, S.J., Stone, J., 1999. Soil erosion by surface water flow on a stony, semiarid hillslope. Earth Surface Processes and Landforms 24 (8), 677–686. https://doi.org/10.1002/(SICI)1096-9837(199908)24:8<677::AID-ESP981>3.3.CO;2-T.

Nearing, M.A., Polyakov, V.O., Nichols, M.H., Hernandez, M., Li, L., Zhao, Y., Armendariz, G., 2017. Slope–velocity equilibrium and evolution of surface roughness on a stony hillslope. Hydrology and Earth System Sciences 21 (6), 3221–3229. https://doi.org/10.5194/hess-21-3221-2017.

Nicosia, A., Di Stefano, C., Palmeri, V., Pampalone, V., Ferro, V., 2020. Flow resistance of overland flow on a smooth bed under simulated rainfall. Catena 187, 104351. https://doi.org/10.1016/j.catena.2019.104351.

Pan, C., Shangguan, Z., 2006. Runoff hydraulic characteristics and sediment generation in sloped grassplots under simulated rainfall conditions. Journal of Hydrology 331 (1–2), 178–185. https://doi.org/10.1016/j.jhydrol.2006.05.011.

Pan, C., Ma, L., Wainwright, J., Shangguan, Z., 2016. Overland flow resistances on varying slope gradients and partitioning on grassed slopes under simulated rainfall. Water Resources Research 52 (4), 2490–2512. https://doi.org/10.1002/2015wr018035.

Polyakov, V., Nearing, M.A., Stone, J., 2018. Velocities of shallow overland flow on semiarid hillslopes. Earth Surface Processes and Landforms 43 (12), 2578–2583. https://doi.org/10.1002/esp.4416.

Powell, D.M., 2014. Flow resistance in gravel-bed rivers: Progress in research. Earth-Science Reviews 136 (1), 301–338. https://doi.org/10.1016/j.earscirev.2014.06.001.

Rahma, A.E., Wang, W., Tang, Z., Lei, T., Warrington, D.N., Zhao, J., 2017. Straw mulch can induce greater soil losses from loess slopes than no mulch under extreme rainfall conditions. Agricultural and Forest Meteorology 232, 141–151. https://doi.org/10.1016/j.agrformet.2016.07.015.

Revell, N., Lashford, C., Rubinato, M., Blackett, M., 2022. The impact of tree planting on infiltration dependent on tree proximity and maturity at a clay site in Warwickshire. England. Water 14 (6), 892. https://doi.org/10.3390/w14060892.

Shang, H., Zhang, K., Wang, Z., Yang, J., He, M., Pan, X., Fang, C., 2020. Effect of varying wheatgrass density on resistance to overland flow. Journal of Hydrology 591, 125594. https://doi.org/10.1016/j.jhydrol.2020.125594.

Shao, S., Luo, M., Rubinato, M., Zheng, X., Pu, J.H., 2020. Advances in Modelling and Prediction on the Impact of Human Activities and Extreme Events on Environments. Water, ISBN 978-3-03936-802-0 (Hbk); ISBN 978-3-03936-803-7 (PDF), 10.3390/books978-3-03936-803-7.

Takken, I., Govers, G., 2000. Hydraulics of interrill overland flow on rough, bare soil surfaces. Earth Surface Processes and Landforms 25 (3), 1387–1402. https://doi.org/10.1002/1096-9837(200012)25:13<1387::AID-ESP135>3.3.CO;2-4.

van Wesenbeeck, B.K., Van De Koppel, J., Herman, P.M.J., Bouma, T.J., 2008. Does scale-dependent feedback explain spatial complexity in salt-marsh ecosystems? Oikos 117 (1), 152–159. https://doi.org/10.1111/j.2007.0030-1299.16245.x.

Wang, W.J., Huai, W.X., Thompson, S., Katul, G.G., 2015. Steady nonuniform shallow flow within emergent vegetation. Water Resources Research 51 (12), 10047–10064. https://doi.org/10.1002/2015wr017658.

Wang, W.J., Peng, W.Q., Huai, W.X., Katul, G.G., Liu, X.B., Qu, X.D., Dong, F., 2019a. Friction factor for turbulent open channel flow covered by vegetation. Scientific Reports 9, 5178. https://doi.org/10.1038/s41598-019-41477-7.

Wang, W.J., Cui, X.Y., Dong, F., Peng, W.Q., Zhen, H., Huang, A.P., Chen, X.K., Si, Y., 2020. Predictions of bulk velocity for open channel flow through submerged vegetation. Journal of Hydrodynamics 32, 795–799. https://doi.org/10.1007/s42241-020-0040-2.

Wang, J.W., Lv, X.R., Zhang, K.D., Li, P., Meng, H., 2019b. Unsteady-State Hydraulic Characteristics of Overland Flow. Journal of hydrologic engineering 24 (10), 04019046.1–04019046.16. https://doi.org/10.1061/(ASCE)HE.1943-5584.0001831.

Wu, F., 2008. Characteristics of Flow Resistance in Open Channels with Non-Submerged Rigid Vegetation. Journal of Hydrodynamics 20 (2), 239–245. https://doi.org/10.1016/s1001-6058(08)60052-9.

Wu, B., Wang, Z., Zhang, Q., Shen, N., Liu, J., 2017. Modelling sheet erosion on steep slopes in the loess region of China. Journal of Hydrology,553:549-558. https://doi.org/10.1016/j.jhydrol.2017.07.017.

Xu, X.Z., Ma, Y.L., Yang, W.J., Zhang, H.W., Tarolli, P., Jiang, Y.Z., Yan, Q., 2020. Qualifying mass failures on loess gully sidewalls using laboratory experimentation. Catena 188, 104252. https://doi.org/10.1016/j.catena.2019.104252.

Yang, P., Zhang, H., Wang, Y., Wang, Y., Wang, Y., 2020. Overland flow velocities measured using a high-resolution particle image velocimetry system. Journal of Hydrology 590, 125225. https://doi.org/10.1016/j.jhydrol.2020.125225.

Zhang, K.D., Wang, G.Q., Sun, X.M., Wang, J.J.,2012. Hydraulic characteristic of overland flow under different vegetation coverage. Advances in Water Science, 2014, 25(6):825-834. (in Chinese). 10.14042/j.cnki.32.1309.2014.06.009.

Zhang, G.H., Luo, R.T., Ying, C., Shen, R.C., Zhang, X.C., 2010. Correction factor to dye-measured flow velocity under varying water and sediment discharges. Journal of Hydrology 389 (1–2), 205–213. https://doi.org/10.1016/j.jhydrol.2010.05.050.

Zhang, H.Y, Zhang, K. D, Liu, L.L, Wang, M., Cen, Y.D., 2022. Quantifying the effects of grass distribution patterns on the relative hydrodynamic parameters of overland flow. Hydrological Processes 36 (10), e14707. https://doi.org/10.1002/hyp.14707.

Zhao, C., Gao, J., Huang, Y., Wang, G., Zhang, M., 2015. Effects of vegetation stems on hydraulics of overland flow under varying water discharges. Land Degradation & Development 27 (3), 748–757. https://doi.org/10.1002/ldr.2423.

Zong, L., Nepf, H., 2010. Flow and deposition in and around a finite patch of vegetation. Geomorphology 116 (3–4), 363–372. https://doi.org/10.1016/j.geomorph.2009.11.020.